



## Prognosis and immunotherapy significances of a cancer-associated fibroblasts-related gene signature in lung adenocarcinoma

Yanli Luo, Sheng Zhang, Huilin Xie, Qiaofeng Su, Shuang He, Zhen Lei\*

Department of Respiratory and Critical Care Medicine, Affiliated Hospital of North Sichuan Medical College, Nanchong, 637002, China

### ARTICLE INFO

#### Original paper

#### Article history:

Received: March 22, 2023

Accepted: September 05, 2023

Published: December 20, 2023

#### Keywords:

Cancer-associated fibroblasts, Immune infiltration, Lung adenocarcinoma, Prognosis, Risk model

### ABSTRACT

Cells associated with cancer (CAFs) contribute significantly to the stroma of a tumor microenvironment (TME), which is related to the occurrence, treatment, and prognosis of lung adenocarcinoma (LUAD). Therefore, this study investigated the function of CAF-associated genes in the microenvironment of LUAD. The Cancer Genome Atlas (TCGA) database was used to download RNA-seq data from the TCGA Lung Adenocarcinoma cohort (TCGA-LUAD). The GSE68465 dataset, as the external validation set, was from the Gene Expression Omnibus (GEO) database. Besides, CAF-associated genes were sourced from the GeneCards and Molecular Signatures Database (MsigDB). For LUAD, differentially expressed CAF-related genes were selected from overlapping CAF and LUAD patient and control samples. Next, LASSO and Univariate Cox analyses were used to construct the risk model. Additionally, an analysis of Cox regression was used to construct a nomogram. Next, the immune infiltration in malignant tumour tissues was compared between high- and low-risk groups using Estimation of STromal and Immune cells in Malignant Tumours (ESTIMATE) tissues and Cell-type Identification by Estimating Relative Subsets of RNA Transcripts (CIBERSORT). The sensitivity differences of immunotherapy between the two risk groups were estimated by Tumor Immune Dysfunction and Exclusion (TIDE), and compared by rank-sum test. Finally, the model genes were detected by fluorescent real-time quantitative polymerase chain reaction (qRT-PCR). A total of 57 DE-CAFGs were acquired, and 9 of them (SHCBP1, CCNA2, AKAP12, CCNB1, GALNT3, SCGB1A1, CPS1, CDC6, and CXCL13) were selected as prognostic biomarkers. The Cox independent prognosis revealed the RiskScore and Stage were the two LUAD independent prognosis factors. Moreover, 11 types of immune cells (memory B cells, resting natural killer cells (NK cells), Eosinophils, Macrophages M0, CD4 memory resting T cells, CD4 memory activated T cells, resting Mast cells, naive B cells, T cells regulatory (Tregs), neutrophils, and plasma cell), and 18 human leukocyte antigen (HLA) genes were different with the two risk groups. Lastly, the TIDE analysis showed differences between the two risk groups for TIDE, T cell dysfunction, and T cell exclusion, PD-L1 treatment scores. Lastly, Both LUAD and normal samples expressed the 9 model genes differently. A CAF-related prognostic model was constructed, which may have potential immunotherapy guiding significance for LUAD patients.

Doi: <http://dx.doi.org/10.14715/cmb/2023.69.14.9>

Copyright: © 2023 by the C.M.B. Association. All rights reserved.

### Introduction

The most common type of cancer and a major cause of cancer-related death is lung cancer (1). Statistics show that in 2018, Nearly 18.4% of deaths caused by cancer were caused by lung cancer (2). Studies have concluded that lung adenocarcinoma (LUAD) is a highly heterogeneous molecular disease and a major pathological subtype of lung cancer with a 5-year survival rate p averaging only 15% (3,4). Most LUAD patients are diagnosed at an advanced stage because the disease is prone to early metastasis, which may be an important reason for the high mortality rate (5,6). Molecular mechanisms, diagnosis and treatment of LUAD have made very important clinical advances, but its recurrence rate remains high and survival rates remain lower than expected (7). Current applied methods still difficult to accurately assess the level of prognosis of patients with LUAD (8). Therefore, improving the accuracy of individual assessment and survival of LUAD patients

remains a top priority in current y research. The development of more efficient and accurate biomarkers to develop optimal personalized treatment and management plans remains a task of urgent research.

Cancer-associated fibroblasts (CAFs) arise and pathologize from different origins, the majority of mesenchymal cells originate from and are recruited by cancerous cells (9). Tumor cells and stromal components, including lymphocytes, neutrophils, plasma cells, endothelial cells, and extracellular matrix (ECM), are surrounded by CAFs. Fibroblasts consist of CAFs, resting fibroblasts, myofibroblasts, and pericytes, and are a source of growth factors, chemokines, cytokines, and other regulatory molecules associated with cancer growth metastasis, angiogenesis, immune effects, and treatment resistance (10). CAFs can influence cancer metastasis and angiogenesis by altering the ECM and promoting growth factors, and influencing the subsequent therapeutic response. CAFs are also important in regulating tumor immunity, promoting immune

\* Corresponding author. Email: [jinzhi4969799@163.com](mailto:jinzhi4969799@163.com)

escape and resisting cancer immunotherapy. Moreover, there is a wide variety of tissue origins, phenotypes, functions, and presences within tumors among CAFs (11-13), but their function in the LUAD microenvironment has not been fully clarified. Targeted CAFs are a promising cancer treatment. However, the future treatment of CAFs in LUAD still has a long way to go.

We downloaded RNA-seq data from the Cancer Genome Atlas Lung Adenocarcinoma (TCGA-LUAD) cohort via the Cancer Genome Atlas (TCGA). Besides, CAF-associated genes were sourced from geneCards and Molecular Signatures Database (MsigDB). This was followed by screening for differentially expressed CAF-associated genes (DE-CAFGs) in LUAD. We then identified 1 nine genes using least absolute shrinkage and selection operator (LASSO) regression analysis to assess the risk score of LUAD based on their expression as an independent prognostic factor. Next, high-risk versus low-risk immune infiltration was investigated by using expression data to estimate stromal and immune cells in Malignant Tumour tissues (ESTIMATE) and by estimating relative subsets of RNA transcripts for cell type identification (CIBERSORT). Finally, differences in sensitivity against immunotherapy between the two groups were assessed by the Tumor Immune Dysfunction and Exclusion (TIDE) method. A nine-gene CAFs-associated risk profile associated with LUAD included immune checkpoints, immune cells, and immunotherapy.

## Materials and Methods

### Data source

The TCGA-LUAD cohort RNA-seq data from the TCGA database contain 535 LUAD tissues and 59 normal tissues. After excluding samples with incomplete survival information or clinical information, 479 LUAD samples were selected for screening prognostic genes and building a prognostic model. Moreover, the GSE68465 dataset, the external validation set, was sourced from the GEO database, including expression profile data of 442 LUAD samples with survival information. 4115 CAF-related genes were retrieved from Gene Cards with the keyword of “cancer-associated fibroblast”, and the screening criteria of “Category = Protein Coding, Relevance score > 2”. Furthermore, the MsigDB database was further used for the search of “fibroblast”, and 279 CAF-related genes were acquired.

### Screening of differentially expressed CAF-related genes in LUAD

Firstly, the differential expression analysis was employed between the 59 normal samples and 535 LUAD samples to screen out the DEGs in LUAD by limma R package (version 3.44.3) (14) with statistical significance  $p$ -value < 0.05 and  $|\text{Log}_2\text{FC}| > 0.5$ . Then, the screened DEGs were further intersected with the 4115 CAF-related genes from GeneCards and 279 CAF-related genes from MsigDB by VennDiagram to obtain CAF-Related Genes (DE-CAFGs) in LUAD, and the result was visualized to the Venn diagram.

### Construction and validation of prognosis model based on DE-CAFGs

Initially, based on the ratio of 7: 3, 336 and 143 samples

of the 479 LUAD samples were treated as training set and internal validation set. Moreover, after extracting DE-CAFGs from the training set, the overall survival (OS) and other clinic information were combined with the extracted expression data to further obtain clinical expression data of LUAD samples. Next, the risk model was taken by univariate Cox analysis and LASSO regression analysis. In detail, univariate Cox measured the survival-related DE-CAFGs with  $p < 0.05$  through survival (version 3.2-3) package (15). LASSO logistic regression analysis was employed by Glmnet (version 4.1-1) (16) with the setting: famil to Cox, to the DE-CAFGs for constructing the risk model. Moreover, the risk score of each LUAD patient was computed by the risk coefficient obtained by the LASSO and the model genes expression levels, with the formula:  $\text{Riskscore} = \sum_1^n \text{coef}(\text{genei}) * \text{expression}(\text{genei})$ , which aimed to examine the prognostic value of the risk model. The overall survival curves were plotted for LUAD patients in both high- and low-risk groups which were nominated based on whether their risk scores were greater than the median value by Survminer (version 0.4.8). Risk further assessed model efficacy using the AUC of ROC curves. Next, The ROC curves of 1, 3, 5 years survival time node were plotted by the survival ROC package (version 3.1-12) to the risk model. Moreover, to determine risk model, the same evaluation procedures were used to evaluate both internal and external validation sets (GSE68465).

### Establishment of a nomogram

To detect the prognosis value of the risk model and clinical factors, the correlation analysis was performed between clinicopathological characteristics (Age, T, N, M, Gender, Smoking-Category, Vital and Stage) of 479 LUAD samples and the risk score. The differences in subgroups of clinicopathological characteristics (M (M0, M1), Age (>65 and =65), T (T1, T2, T3, T4), Gender (Male, Female), Smoking-Category (Non-Smoker, Smoker), N (N0, N1, N2, N3), Vital (Alive, Dead)) between the two risk groups were examined by Chi-square test. Additionally, the rank-sum test was further utilized to compare differences in risk scores among the different subgroups of clinicopathological characteristics. Furthermore, the K-Msurvival curve was further employed to the clinicopathological characteristics in high- or low-risk groups of risk score to inspect the survival probabilities between the two groups in different subgroups of the clinicopathological characteristics.

Next, the univariate Cox analysis was further employed to the clinicopathological characteristics and RiskScore of 479 LUAD samples to investigate the characteristics and the risk model. Subsequently, the clinicopathological characteristics with  $p < 0.05$  were considered as the factors for the subsequent multivariate Cox independent prognostic analysis.

Then, the rms function (version 6.2-0) in the R package was employed on the 479 LUAD samples to build the nomogram to further predict LUAD patients 1, 3, and 5-year survival probabilities according to the total score of independent factor screened by the Cox analyses, and the nomogram was verified by the overall calibration curve. In addition, the effectiveness of the risk model and nomogram was further evaluated by Decision Curve Analysis (DCA) curves, which aimed to compare the prediction accuracies.

**Table 1.** Primers for qPCR.

Primer	Sequence
SHCBP1 F	GAGCCTGGTGAGGAAGAAAGAG
SHCBP1 R	CAATGGAGTCAGCAATGGAGAA
CCNA2 F	CCATTCATGTGGATGAAGCAGAA
CCNA2 R	CCATTGGATAATCAAGAGGGACC
AKAP12 F	CATGAGGAGAATGAGGTGCGC
AKAP12 R	AAACTGGAAGGTGCTGGAGG
CCNB1 F	TTTAAACTTTGGTCTGGGTCGG
CCNB1 R	CTGCTGCAATTTGAGAAGGAGG
GALNT3 F	ATACAGCAGCAGAATTGAAGCC
GALNT3 R	TGCAGGTGAAGAATAGAGCAC
CPS1 F	GTCTACTTTCTCCCATCACCCC
CPS1 R	CATATTCCTTGAGCACACCTCTC
CDC6 F	GGAGATGTTTCGCAAAGCACTG
CDC6 R	AACCCTCTTGGGAATCAGAGG
CXCL13 F	GCTTGAGGTGTAGATGTGTCC
CXCL13 R	CCCACGGGGCAAGATTTGAA
SCGB1A1 F	GATCAAGACATGAGGGAGGCAG
SCGB1A1 R	ACACAGTGAGCTTTGGGCTATT
GAPDH F	CCCATCACCATCTTCCAGG
GAPDH R	CATCACGCCACAGTTTCCC

### Effects of risk model on immune heterogeneity

CIBERSORT (version 1.03) (17) analyzes the immune cell infiltration landscape of 479 LUAD samples. In the current study, the LM22 signature computes the corresponding proportion of each type of immune cell in each LUAD sample. In addition, the estimate package (version 1.0.13) was performed on the 479 LUAD samples to detect the immune infiltration differences. The immune infiltration of both immune and stromal cells in a tumor sample can be obtained by the ESTIMATE algorithm, which would be presented as stromal scores, immune scores, and ESTIMATE composite scores. Then, Spearman analysis was employed to discover the correlations in risk scores with stromal scores, immune scores, and ESTIMATE composite scores. Furthermore, the proportion of CAF in each LUAD sample can be obtained by McP-counter, xCell, TIDE and EPIC, and Spearman was further applied to distinguish the relation between risk score and CAF proportion.

Moreover, the 19 human leukocyte antigen (HLA) genes obtained from the publication of Yue et al. (18), were extracted from the LUAD expression matrix. The 22 cancer-associated fibroblasts (CAF) markers were acquired from the research of Zheng et al. (19), and 8 chemokines/cytokines were obtained based on Chen et al. (20) (Supplementary Table 1). The expression differences of 19 HLA genes, 22 CAF markers, and 8 chemokine/cytokine between the two risk groups were analyzed through rank-sum test. Risk model genes were correlated with HLA genes, CAF markers, and chemokine/cytokine levels using Spearman analysis.

### Analyses of immunotherapy response

The TIDE method was used to determine whether immunotherapy sensitivity differed between the two risk groups. TIDE was used to obtain the TIDE, T cell dysfunction, T cell exclusion, and PD-L1 (AKA CD274) treatment

scores of each LUAD sample, and the rank-sum test investigated the differences of the 4 scores between both risk groups. In addition, the chi-square test was employed separately in the two risk groups to compare the numbers of people with response and no response to immunotherapy.

### Real-time qPCR

Total RNA was extracted by lysing LUAD samples with TRIzol reagent (Life Technologies, CA, USA). qualified RNA was reverse transcribed to cDNA and using the 2- $\Delta\Delta C_t$  method in the BIO-RAD CFX96 Touch TM PCR Detection System (Bio-Rad Laboratories, Inc., USA). All experiments were approved by the ethics committee after informed consent was obtained from subjects. The primer sequences used were as follows (Table 1).

### Results

#### Identifications of DE-CAFGs

Five hundred and thirty-five LUAD samples and sixty-nine normal samples provided 3709 DEGs, which included 2163 raised and 1546 dropped genes (Figure 1A). Moreover, the overlap construe results between 3709 DEGs and CAF-related genes showed that 57 DE-CAFGs were finally obtained (Figure 1B) (Supplementary Table 2).

#### An effective risk model based on 9 model genes was developed

The expression data of 57 DE-CAFGs were extracted from the training set. After combining with OS clinical information, a forest map was drawn to visualize the univariate Cox analysis results, as can be seen that 9 DE-CAFGs relevant to survival were screened out including SHCBP1, CCNA2, AKAP12, CCNB1, GALNT3, SCGB1A1, CPS1, CDC6, and CXCL13. Besides, SCGB1A1 and CXCL13 were the protection factors ( $HR < 1$ ) and the rest 7 of them were risk factors ( $HR > 1$ ) (Figure 2A). The LASSO regression analysis of 9 DE-CAFGs relevant to survival results suggested these 9 genes were screened out as model genes when the cross-validation error was lowest ( $\lambda_{min} = 0.00355$ ) (Figure 2B) (Table 2). The risk score of the 9 model genes =  $0.34891 \times SHCBP1 + 0.16841 \times CCNA2 + 0.15019 \times AKAP12 + 0.24073 \times CCNB1 + 0.20254 \times GALNT3 + 0.04754 \times CPS1 + (-0.00943) \times SCGB1A1 + (-0.47551) \times CDC6 + (-0.11165) \times CXCL13$ . Using the risk score, the risk curve revealed that high-risk patients had poor survival rates (Figure 2C). The K-M curve illustrated that the low-risk patients had a higher survival probability ( $p < 0.0001$ ) (Figure 2D). Furthermore, one-

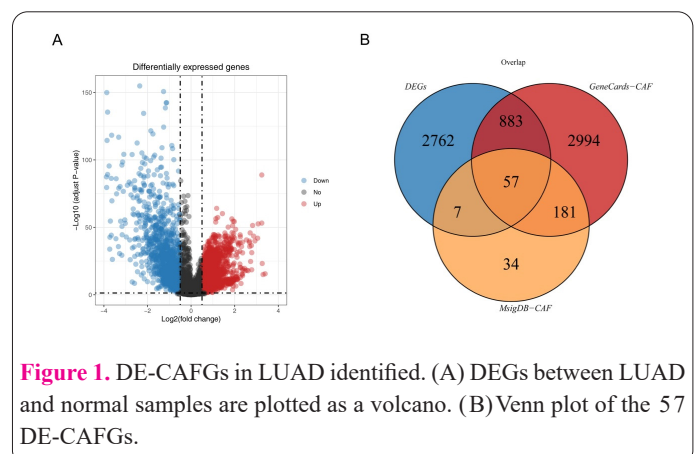


**Figure 1.** DE-CAFGs in LUAD identified. (A) DEGs between LUAD and normal samples are plotted as a volcano. (B) Venn plot of the 57 DE-CAFGs.

**Table 2.** Risk model gene risk coefficient.

Gene	Coef	Exp(coef)	Se(coef)	Z	P
SHCBP1	0.34891	1.41752	0.21163	1.649	0.0992
CCNA2	0.16841	1.18342	0.20016	0.841	0.4001
AKAP12	0.15019	1.16206	0.07511	2	0.0455
CCNB1	0.24073	1.27218	0.19392	1.241	0.2145
GALNT3	0.20254	1.2245	0.08258	2.453	0.0142
SCGB1A1	-0.00943	0.99061	0.03051	-0.309	0.7573
CPS1	0.04754	1.04868	0.03419	1.39	0.1645
CDC6	-0.47551	0.62157	0.18477	-2.574	0.0101
CXCL13	-0.11165	0.89436	0.05075	-2.2	0.0278

, three-, and five-year ROC curves all had AUCs better than 0.6, revealing that the risk model was efficient (Figure 2E). Moreover, both internal and external validation (GSE68465) sets all showed consistent results with that of the training set (Figure 2F - 2K).

**Clinical correlation analysis**

The Chi-square test result suggested there were differences in the T, N, M, Gender, Vital and Stage between the two risk groups, except for Smoking-Category ( $p = 0.46$ )

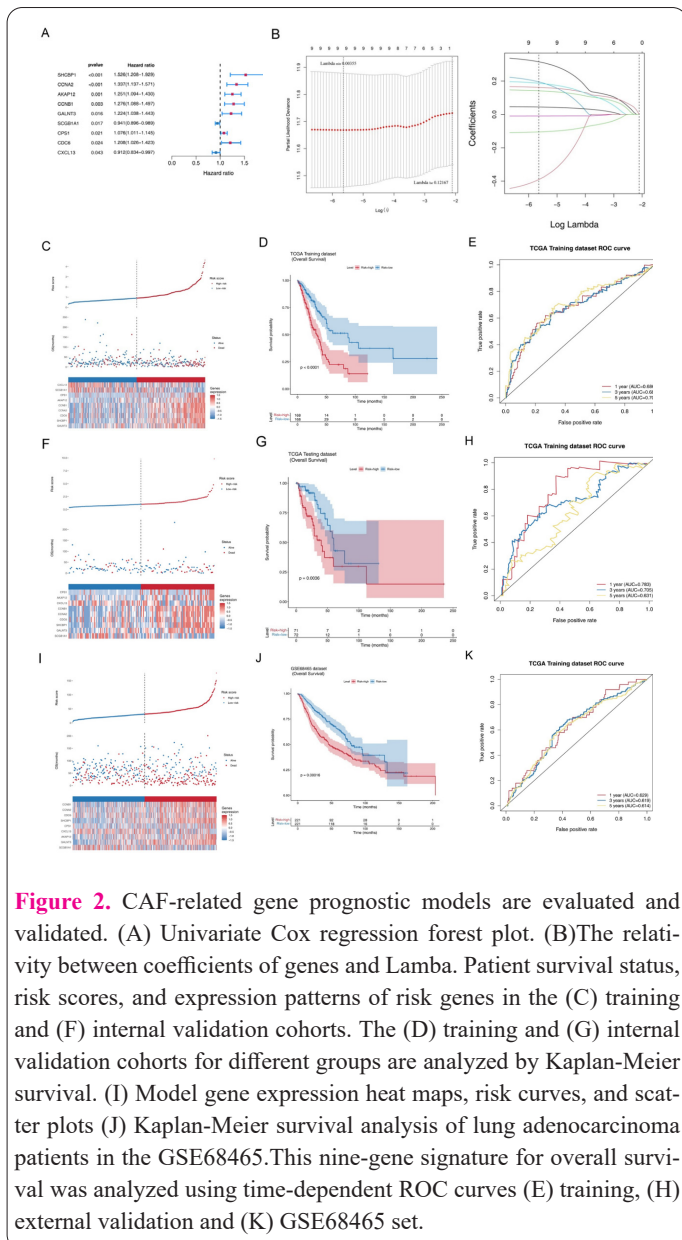


**Figure 2.** CAF-related gene prognostic models are evaluated and validated. (A) Univariate Cox regression forest plot. (B)The relationship between coefficients of genes and Lambda. Patient survival status, risk scores, and expression patterns of risk genes in the (C) training and (F) internal validation cohorts. The (D) training and (G) internal validation cohorts for different groups are analyzed by Kaplan-Meier survival. (I) Model gene expression heat maps, risk curves, and scatter plots (J) Kaplan-Meier survival analysis of lung adenocarcinoma patients in the GSE68465. This nine-gene signature for overall survival was analyzed using time-dependent ROC curves (E) training, (H) external validation and (K) GSE68465 set.

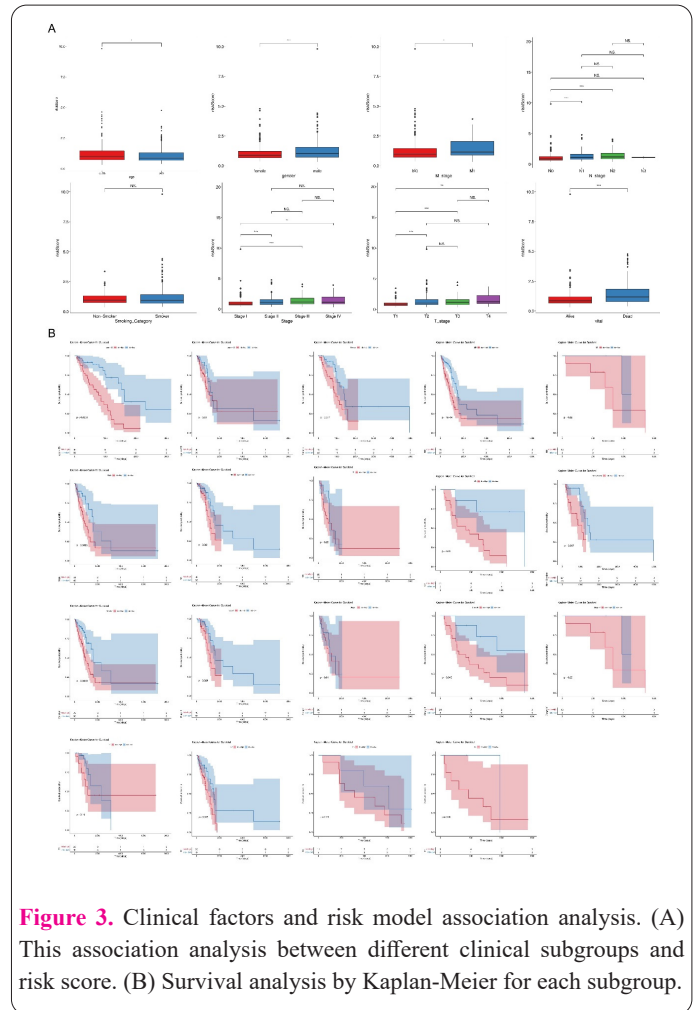


**Figure 3.** Clinical factors and risk model association analysis. (A) This association analysis between different clinical subgroups and risk score. (B) Survival analysis by Kaplan-Meier for each subgroup.

and Age ( $p = 0.051$ ) (Table 3). Furthermore, the rank-sum test results demonstrated the risk score differences among the subgroups of T, N, M, Stage, Age, and Gender groups were significant (Figure 3A). Moreover, the stratified survival analysis of the clinical factors showed survival differences between the risk groups among the subgroups in M (M0), Age, T (T2), Gender, Smoking-Category, N (N0, N2), and Stage (StageI/StageIII/StageIV) (Figure 3B).

**Prediction of the nomogram was accurate**

The univariate Cox independent prognostic analysis result illustrated T, N, M, stage, and risk score could be considered as prognosis factors ( $p < 0.05$ ) (Figure 4A). Next, the Multivariate Cox independent prognostic revealed the stage ( $p = 0.037$ ), and the independent prognostic element for LUAD is the risk score ( $p < 0.001$ ), and LUAD risk models constructed in this study were found to be reliable independent prognostic elements (Figure

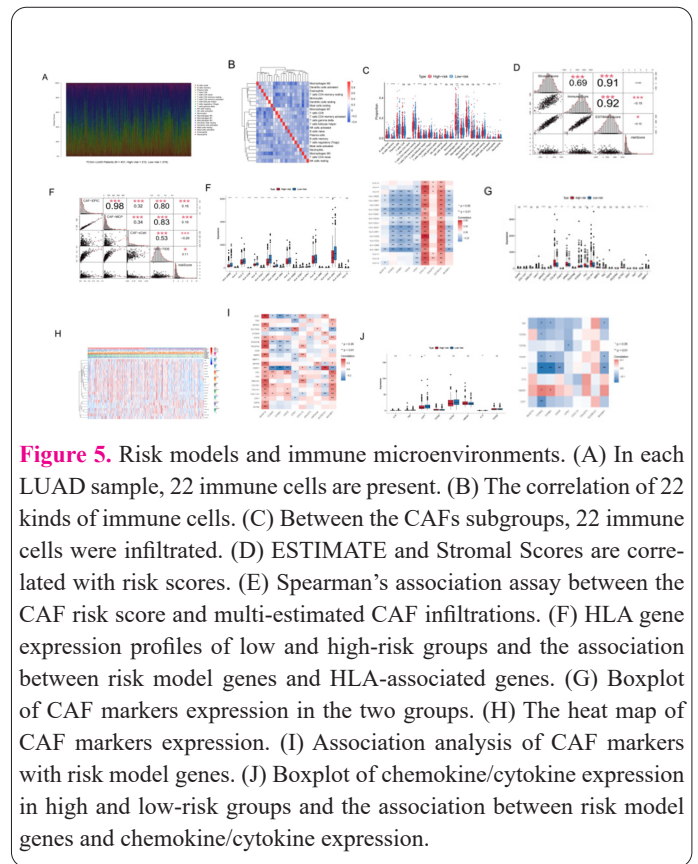
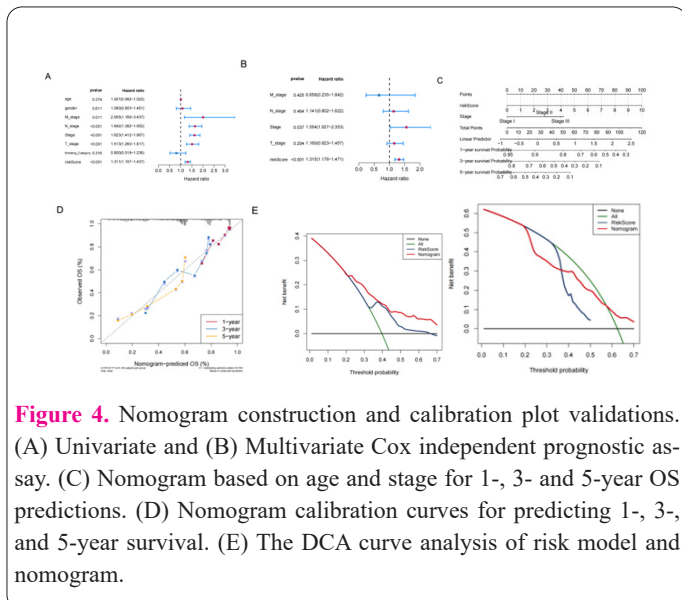
**Table 3.** Risk and clinical data.

Characteristics	Total	Risk		P-value	
		High	Low		
Age (year)	65.3 (±10.1)	64.5 (±10.5)	66.1 (±9.5)	0.051	
mean (SD)					
Gender	female	260 (54.3%)	111 (46.4%)	149 (62.1%)	<0.001
	male	219 (45.7%)	128 (53.6%)	91 (37.9%)	
Vital	alive	302 (63.0%)	127 (53.1%)	175 (72.9%)	<0.001
	dead	177 (37.0%)	112 (46.9%)	65 (27.1%)	
Stage	I	259 (54.1%)	104 (43.5%)	155 (64.6%)	<0.001
	II	117 (24.4%)	67 (28.0%)	50 (20.8%)	
	III	78 (16.3%)	50 (20.9%)	28 (11.7%)	
	IV	25 (5.2%)	18 (7.5%)	7 (2.9%)	
M Stage	M0	316 (92.9%)	164 (90.1%)	152 (96.2%)	0.034
	M1	24 (7.1%)	18 (9.9%)	6 (3.8%)	
N Stage	N0	311 (66.2%)	136 (57.6%)	175 (74.8%)	<0.001
	N1	90 (19.1%)	56 (23.7%)	34 (14.5%)	
	N2	67 (14.3%)	43 (18.2%)	24 (10.3%)	
	N3	2 (0.4%)	1 (0.4%)	1 (0.4%)	
Smoking Category	non-smoker	58 (21.7%)	32 (23.7%)	26 (19.7%)	0.46
	smoker	209 (78.3%)	103 (76.3%)	106 (80.3%)	
T Stage	T1	164 (34.5%)	57 (23.9%)	107 (45.0%)	<0.001
	T2	251 (52.7%)	142 (59.7%)	109 (45.8%)	
	T3	44 (9.2%)	26 (10.9%)	18 (7.6%)	
	T4	17 (3.6%)	13 (5.5%)	4 (1.7%)	

4B). Moreover, the C-index of the nomogram stage and risk score was 0.7008, and the slopes of patients overall survival in one-year, three-year and five-year were close to 1, revealing that the prediction was exact (Figure 4C, 4D). Moreover, DCA curves also suggest that the net benefit of the nomogram was greater than the risk model (Figure 4E).

**Correlation between risk model and tumor microenvironment**

CIBERSORT was used to investigate the immune cells in 431 LUAD samples (HIGH = 219, LOW = 212) after eliminating samples with p>0.05 (Figure 5A). It can be



found that 22 kinds of immune cells negatively regulate each other, and 11 kinds of immune cells (eosinophils, B cell memory, macrophage M0, B cell immature, T cell CD4 memory resting, plasma cells, NK cell resting, T cell regulation (Treg), T cell CD4 memory activation, mast cell

**Table 4.** Expression levels of 9 model genes by RT-qPCR.

	NC	Ca	T, df value	P value
CPS1	1.0452±0.0284	4.0835±2.0552	t=3.273 df=4	0.0307
AKAP12	1.0003±0.0005	0.4090±0.0581	t=22.75 df=4	<0.0001
CXCL13	1.0008±0.0013	4.1521±0.2707	t=25.93 df=4	<0.0001
CCNB1	1.0008±0.0007	4.9066±1.2854	t=6.794 df=4	0.0025
CCNA2	1.0023±0.0026	5.3770±1.5139	t=6.461 df=4	0.003
CDC6	1.0213±0.0315	3.7492±1.0503	t=5.888 df=4	0.0042
SHCBP1	1.0063±0.0107	2.9231±0.5386	t=8.105 df=4	0.0013
GALNT3	1.0031±0.0027	5.6367±1.1312	t=9.173 df=4	0.0008
SCGB1A1	1.0037±0.0018	0.4173±0.1554	t=8.469 df=2	0.0011

quiescence, and neutrophils) were different between the 2 risk groups (Fig. 5B, 5C). Then, In the Spearman analysis, EPIC, xCell, and McP-counter CAF ratios showed a correlation with risk score ( $p < 0.05$ ) (Figure 5E).

In addition, the HLA gene revealed 18 HLA genes (DRB5, F, C, DOB, E, DQA1, DRB1, DPB1, DMA, A, DQB2, DQB1, DPA1, B, DMB, DOA, DRA, DQA2) significantly differentially expressed between the two risk groups, and the risk model genes were strongly correlated with the 19 HLA genes (Figure 5F). 10 CAF markers (COL11A1, MFAP5, COL3A1, FOXF1, SPARC, FN1, COL1A1, FAP, OGN, and MMP11) expressed differentially between the two groups (Figure 5G, 5H), and CAF markers showed strong positive/negative correlation with risk model genes (Figure 5I). Besides, the analysis of 8 chemokines/cytokines illustrated that the expressions of 3 of TNF, CSF1 and IL13 were significantly different between risk groups, and there were strongly negative correlations between risk model genes and chemokines/cytokines (Figure 5J).

### Analysis of immunotherapy differences

The variation in sensitivity of immunotherapy in the two groups was assessed using TIDE. It can be found that T cell dysfunction, PD-L1 and T cell excluded, treatment scores all showed variation between the two risk groups, and the TIDE score was greater in a high-risk group, which indicated the efficacy of immune checkpoint blocking (ICB) therapy was poor in the high-risk group (Figure 6A). Additionally, the chi-square test result demonstrated

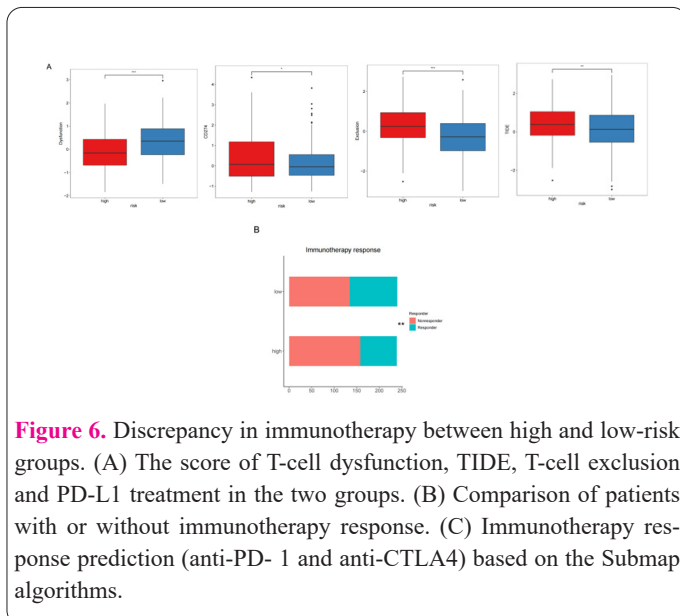


**Figure 6.** Discrepancy in immunotherapy between high and low-risk groups. (A) The score of T-cell dysfunction, TIDE, T-cell exclusion and PD-L1 treatment in the two groups. (B) Comparison of patients with or without immunotherapy response. (C) Immunotherapy response prediction (anti-PD-1 and anti-CTLA4) based on the Submap algorithms.

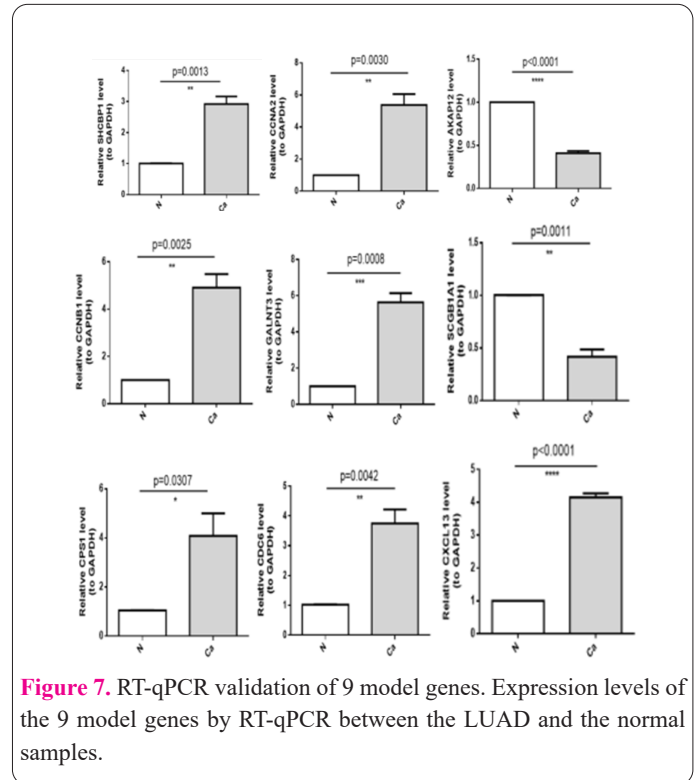


**Figure 7.** RT-qPCR validation of 9 model genes. Expression levels of the 9 model genes by RT-qPCR between the LUAD and the normal samples.

that there were differences in the numbers of nonresponders and responders between the risk groups, which were significantly more responders in this low-risk group (Figure 6B).

### RT-qPCR validation of 9 model genes

For further verification of the 9 model genes' expression levels (SHCBP1, CCNA2, AKAP12, CCNB1, GALNT3, SCGB1A1, CPS1, CDC6, CXCL13), RT-qPCR was performed in 5 pairs of LUAD samples. It can be found that the 9 model genes were different between the LUAD and the normal samples (all  $P < 0.05$ ). Consistent with TCGA results, the AKAP12 and SCGB1A1 were significantly lower in LUAD samples, and all the rest 7 model genes (CPS1, CXCL13, CCNB1, CCNA2, CDC6, SHCBP1, and GALNT3) were raised in LUAD in comparison with normal samples. Therefore, these 9 model genes could be considered as the prognosis genes of LUAD (Table 4, Figure 7).

### Discussion

LUAD is a type of non-small cell lung cancer (NS-CLC) that is characterized by high heterogeneity and high

malignancy. (3,21). Due to the complex characteristics of LUAD, efficient prediction of prognosis in patients with LUAD remains challenging (22). Lately, studies targeting the regulation of the immune system by CAFs have received increasing attention. Numerous researches demonstrated that CAFs is important in the progress of cancer (11). Hence, novel CAFs have become a hot point in the realm of cancer and are important biomarkers and key to targeted therapies.

In this research, the LUAD dataset from TCGA databases, and CAF-associated genes, we first screened out 57 DE-CAFGs. The univariate Cox selected 9 DE-CAFGs. Next, a signature of 9 DE-CAFGs predicting OS in LUAD patients was used LASSO Cox regression analysis. Based on our findings, nine CAFs-related genes were possibly correlated with survival outcomes in LUAD. Furthermore, 9 CAFs-related genes (SHCBP1, CCNA2, AKAP12, CCNB1, GALNT3, SCGB1A1, CPS1, CDC6, and CXCL13) were selected as prognostic biomarkers. Among them, CXCL13 and SCGB1A1 are favorable prognostic genes in LUAD patients, while the rest of the seven are adverse prognostic genes. Numerous types of cancer are overexpressed with SHCSH2-binding protein 1 (SHCBP1) (23). The loss of SHCBP1 in hepatocellular carcinoma (HCC) cells inhibits cell proliferation and increases apoptosis (24). As a result of SHCBP1, breast cancer spreads and apoptosis occurs (25). Consistent with our study, according to Wang et al. (23) SHCBP1 in cancerous lungs is significantly higher than in normal lung tissues, suggesting that SHCBP1 could be a candidate lung cancer oncogene. The CCNA2 gene is located on chromosome 4 which belongs to the highly conserved cyclin family. Several studies have demonstrated that this gene may enhance cancer aggressiveness, relapses, and metastases and chemoresistance (26). As reported by Zhou et al. (27) CCNA2 is correlated with immunity therapy efficiency in LUAD and can be used as a diagnostic and prognostic biomarker. As cancer progresses, AKAP12 is downregulated, often due to promoter hypermethylation or its locus at 6q24-25.2 is lost (28,29). In lung cancer tumors, the AKAP12 $\alpha$  promoter is more frequently methylated and is associated with poor prognosis (29,30). A mucin-like O-linked protein including in the proliferation, migration and adhesion of tumor cells is glycosylated by GalNAc-T3. By reducing the production of CXCL1, GALNT3 inhibits the development of lung cancer by blocking the development of myeloid-derived suppressor cells (MDSCs), resulting decrease in angiogenesis (31). In different cancers, GALNT3 can both promote and inhibit tumor progression. It seems even this is controversial since one study found that GALNT3 promoted pancreatic cancer cell growth, but others found that GALNT3 suppressed it (32), and another study showed that GALNT3 suppresses pancreatic cancer (33). GALNT3 is also thought to promote colon cancer (34). Our study suggested that GALNT3 is a tumor-suppressing gene in LUAD. We found that GALNT3 is upregulated in LUAD and related to OS in patients with LUAD. PCR results also confirmed that GALNT3 was overexpressed in LUAD tissues than normal tissue. Furthermore, a urea cycle, CPS1 is a rate-limiting enzyme that promotes proliferation and the growth of tumors (35). CPS1 promotes tumors in LUAD, and high CPS1 has a worse outlook (36). NSCLC driven by epidermal growth factor receptor (EGFR) relies on the CPS1-mediated urea

cycle for growth. It is possible to further reduce the proliferation of NSCLC (non-small cell lung cancer) by inhibiting EGFR once CPS1 is knocked down (37).

Recently, the research on immune cell infiltration in tumors has been increasing attention. The infiltration of immune cells is thought to contribute to the progression of LUAD and colorectal cancer (CRC) and the response to immunotherapy (38,39). There is increasing evidence that tumor immune infiltration levels are related to cancer patient prognosis. There is a relation between immune infiltrating cells and prognosis among LUAD with high- and low-risk scores. In the current study, we know the proportions of 11 immune cells (memory B cells, Eosinophils, naive B cells, Macrophages M0, CD4 memory resting T cells, T cells regulatory (Tregs), Plasma cells, CD4 memory activated T cells, resting NK cells, resting Mast cells, and Neutrophils) were significantly different between 2 risk groups. Cytotoxic T lymphocytes (CTLs) are stimulated in tumors by cancer immunotherapy and activate tumor-specific CTLs in lymphoid organs to establish effective and durable antitumor immunity. CTLs with CD4+ T cells are more effective at fighting tumors (40). As an important innate immune sentinel, mast cells improve the immune response mediated by T cells, however, other examples demonstrate the ability to inhibit immune responses (41,42). Mast cell number in TME is found to be related to cancer development and better patient survival due to their functional plasticity (42). The infiltration of mast cells in tumorislets is independent of the stage of the cancer in NSCLC (43). Further study showed that tumor infiltration by macrophages was associated with tumor lymphatic angiogenesis and worse prognosis in LUAD (44). Kawai et al. (45) mentioned that macrophage infiltration could indicate the prognosis of patients with stage IV NSCLC. As a result, the diversity in survival outcomes between risk groups may be due to the infiltration of immune cells in TME. According to these results, immunotherapy might have better results for patients within the CAFs low-risk group.

Some researches have shown that CAFs are negatively related to LUAD patient prognoses, suggesting that CAFs have a vital role in tumor progression (46,47). The secretion of cytokines and chemokines by CAFs contributes to tumor development and resistance to treatment. Pechkovsky et al. (48) investigated how CAFs are spontaneously expressed in the lung parenchyma using patient-derived samples from the proximal bronchus and distal lung parenchyma of normal people  $\alpha$ -SMA, implying the role of  $\alpha$ -SMA in the development of lung cancer. Simultaneously, it was found that OPN was overexpressed in senescent fibroblasts which were the important mediators to promote tumor growth (48,49). According to Richardson et al. (50) vimentin marker functions through CAFs but not through cancer cells. Invasion and metastasis of lung adenocarcinomas were promoted by vimentin expressed in CAFs. By secretion of SRGN, Through CD44/NF-B/claudin-1 axis recruitment, CAFs improved the EMT of lung cancer cells. Additionally, an article mentioned that CAF-conditioned medium increased vascular Cell adhesion molecule-1 (VCAM-1) in comparison with conditioned medium from normal lung fibroblasts (NLF), thereby increasing the proliferation and metastasis in lung cancer cells (51). By activating AKT and MAPK signaling pathways, VCAM-1 secreted from CAFs promoted tumor growth and invasion

reversibly. CAFs can activate the pi3k/akt/mTOR pathway in non-small cell lung cancer cells through interleukin-22 and significantly promote the migration and invasion of tumor cells (52).

Several pathways enriched in tumors, including epithelial-mesenchymal transformation, were identified (53), hypoxia (54), inflammatory response (55), interferon-gamma response (56) and NFkB-mediated TNF $\alpha$  signal transduction (57) which were correlated to the function of CAFs. An enhanced tumor-promoting ability of CAFs was observed in hypoxia microenvironments. The CAIX index represents hypoxia, which is associated with poor prognosis in patients with lung adenocarcinoma (58). Cancer cells grew aggressively when CAIX (+) CAFs attracted tumor-promoting stromal cells, for instance, CD204 (+) tumor-associated macrophages (TAMs) and podoplanin (+) CAFs. The CAFs in lung adenocarcinoma were upregulated by chemotherapy, radiotherapy, and hypoxia stress and the NF-B/BCL-XL pathway was activated by the compound, resulting in chemoresistance. By reducing cellular ROS levels, GSH increases resistance to death stimuli. In LUAD, CAFs expressed GGT5 predominantly and increased intracellular GSH and reduced ROS levels in lung cancer cells. Low expression of GGT5 promotes the sensitivity of lung cancer cells to paclitaxel and cisplatin. Another study found that CAFs in lung adenocarcinoma after cisplatin treatment conferred drug resistance to lung cancer cells by up-regulating interleukin-11 and activating the STAT3 antiapoptotic pathway. The researchers also suggested that patients with high levels of interleukin-11 receptor expression had poor response to cisplatin (59).

In addition to promoting angiogenesis and recruiting immunosuppressive cells into the TME, CAFs can secrete several growth factors and proinflammatory cytokines (60,61). An immune-suppressed status was more likely to be predicted in high-risk groups. There was a lower infiltration of immune cells and high expression of HLA-I and HLA-II in the high-risk group. It has been found that CAFs in lung cancer tissue can recruit granulocyte-like myeloid suppressor cells into the tumor by secreting chemokines such as CXCL1, cxcl2, CXCL5 and CCL3 to form an immunosuppressive tumor microenvironment (62). Cancer-infiltrating immune cells (TIICs) were induced to differentiate into immune-suppressive cells by CAFs. TMEs may be immunosuppressive when CAFs polarize macrophages to M2 macrophages. MDSCs activated by CAFs suppress CD8<sup>+</sup> T cell proliferation and IFN $\gamma$  production, creating an immunosuppressive tumor microenvironment. A recent study pointed out that CAFs of lung adenocarcinoma can directly interact with activated CD8<sup>+</sup> T cells through antigen presentation and induce T cell death through binding of PD-L2 and Fas ligands. Furthermore, T cells containing antigens were significantly impaired in their ability to kill tumor cells when they were regulated by antigen-loaded CAFs, it appears that CAFs can enhance tumor cell viability by causing tumor-specific T cells to become dysfunctional and die (63). Past studies have proven that CAFs promote the recruitment and differentiation of Treg cells by recruiting and balancing CD4<sup>+</sup> effector T cell subsets (Th1 and Th2). Immune cells that attack tumors innately (NK cells). Researchers found that CAFs reduced the proliferation rate, cytotoxic capacity, and anti-tumor activity of NK cells in vitro, extensive degranulation, as well as promoting the expression of inhibitory receptors

while inhibiting stimulatory receptors (64). It appears that CAFs and their secreted factors promote the progression of LUAD by orchestrating with immune cells within the TME.

TIDE predicts the likelihood of tumor immune escape positively. The results indicate that ICIs are less beneficial for patients with higher TIDE scores. In those research, CAFs with low risk had lower TIDE scores and T cell exclusion scores, while those with high risk had higher TIDE and T cell dysfunction scores. Thus, patients at high risk of CAFs may suffer immune escape because of dysfunctional T cells and respond poorly to ICIs, in contrast, patients at low risk of CAFs may benefit more from ICIs. Low-risk patients are more effective with immunotherapy. The results show that the nine CAFs-related genes can provide a novel and reliable method to estimate a patient's prognosis by calculating a risk score and clinical response to immunotherapy for LUAD. CAFs also altered the expression of immune checkpoints, such as PD-L1, in addition to regulating immunity directly. PD-1 and PD-L1 help tumor cells survive by evading T-cell recognition (65). PD-L1 or PD1 receptor targeting has been shown to be available in treating NSCLC (66). CAFs secrete CXCL2, which significantly increases PD-L1 expression in lung adenocarcinomas, accelerating tumor progression (67). Consequently, CAFs can affect lung cancer patients' immune responses and targeting CAFs could promote immunotherapy's efficacy.

Until now, no study has explored the clinical features of CAFs in LUAD and established a prognostic signature, using CAFs to predict LUAD survival outcomes and immunotherapy effectiveness. Furthermore, nine CAF-related genes should be explored in depth as prognostic markers. Due to LUAD's complex and diverse immune environment, CAFs play different roles in different patients. Therefore, further clarification is needed regarding CAFs' effects on tumor cells and immune cells.

While our study has some limitations, one of the most important is that it was mainly based on bioinformatics analysis. Further systematic experiments are needed to validate our statements since there were few experiments to confirm our findings. In addition, RT-qPCR is performed only to detect differences in expression levels between LUAD samples and controls, which is urgent to explore the functions of the nine genes in LUAD.

## Conclusions

Increased infiltration of CAFs in LUAD is clearly associated with advancing age (age > 65), gender, M0, N0, N2, T2, Stage (I, III, IV), Smoking Category, score of stromal, immune and ESTIMATE and patient prognosis. Prognostic models about nine CAFs-related genes have wide application. Prognosis and immunotherapy response for LUAD patients can be predicted using the risk model.

## Abbreviations

CAF: Cancer-associated fibroblasts, TME: tumor microenvironment, LUAD: lung adenocarcinoma, Tregs: T cells regulatory, HLA: human leukocyte antigen, ECM: extracellular matrix, TCGA-LUAD: the cancer genome atlas lung adenocarcinoma, TCGA: The Cancer Genome Atlas, GEO: Gene Expression Omnibus, MsigDB: molecular signatures database, DE-CAFGs: differentially expressed CAF-related genes, DEGs: differentially expressed genes,

LASSO: least absolute shrinkage and selection operator, ESTIMATE: estimation of stromal and immune cells in malignant tumour tissues using expression data, CIBERSORT: cell-type identification by estimating relative subsets of RNA transcripts, TIDE: tumor immune dysfunction and exclusion, OS: overall survival, AUC: area under curve, ROC: Receiver operating characteristic, KM: Kaplan-Meier, DCA: decision curve analysis, ICB: immune checkpoint blocking, MDSC: myeloid-derived suppressor cells, CRC: colorectal cancer, CTLs: cytotoxic T lymphocytes, VCAM-1: vascular cell adhesion molecule-1, NLF: normal lung fibroblasts, CAIX: carbonic anhydrase IX, TAMs: tumor-associated macrophages, TNFSF4: tumor necrosis factor superfamily member 4, TIIC: tumor-infiltrating immune cells, NK cells: natural killer cells, NSCLC: non-small cell lung cancer, HCC: hepatocellular carcinoma, EGFR: epidermal growth factor receptor.

### Funding

Funding information is not available.

### Authors' contributions

(I) Conception and design: Y Luo, Z Lei; (II) Perform data analysis and write the manuscript: Y Luo, S He, S Zhang, Q Su, H Xie; (III) Revise the manuscript: Y Luo, S Zhang, Z Lei; (V) Final approval of manuscript: All authors.

### Acknowledgements

The authors gratefully acknowledge contributions from the GEO and TCGA network.

### Availability of data and materials

Additional data and materials may be requested from the corresponding author on reasonable request.

### Ethics approval and consent to participate

The study was approved by the Research Ethics Committee of Affiliated Hospital of North Sichuan Medical College, China. All patients provided written informed consent.

### Consent for publication

Not applicable.

### Competing interests

The authors declare that they have no competing interests.

### References

- Siegel RL, Miller KD, Jemal A. Cancer statistics. 2019. *CA Cancer J Clin* 2019; 69(1): 7-34. <https://doi.org/10.3322/caac.21551>
- Bray F, Ferlay J, Soerjomataram I, Siegel RL, Torre LA, Jemal A. Global cancer statistics 2018: GLOBOCAN estimates of incidence and mortality worldwide for 36 cancers in 185 countries. *CA Cancer J Clin* 2018; 68(6): 394-424. <https://doi.org/10.3322/caac.21492>
- The Cancer Genome Atlas Research Network. Author Correction: Comprehensive molecular profiling of lung adenocarcinoma. *Nature* 2018; 559: E12. <https://doi.org/10.1038/s41586-018-0228-6>
- Miller KD, Nogueira L, Mariotto AB, Rowland JH, Yabroff KB, Alfano CM, Jemal A, Kramer JL, Siegel RL. Cancer treatment and survivorship statistics. 2019. *CA Cancer J Clin* 2019; 69: 363-385. <https://doi.org/10.3322/caac.21565>
- Riihimaki M, Hemminki A, Fallah M, Thomsen H, Sundquist K, Sundquist J, Hemminki K. Metastatic sites and survival in lung cancer. *Lung Cancer* 2014; 86: 78-84. <https://doi.org/10.1016/j.lungcan.2014.07.020>
- Bender E. Epidemiology: the dominant malignancy. *Nature* 2014; 513: S2-S3. <https://doi.org/10.1038/513S2a>
- Field JK, Oudkerk M, Pedersen JH, Duffy SW. Prospects for population screening and diagnosis of lung cancer. *Lancet* 2013; 382: 732-741. [https://doi.org/10.1016/S0140-6736\(13\)61614-1](https://doi.org/10.1016/S0140-6736(13)61614-1)
- Calvayrac O, Pradines A, Pons E, Mazières J, Guibert N. Molecular biomarkers for lung adenocarcinoma. *Eur Respir J* 2017; 49: 1601734. <https://doi.org/10.1183/13993003.01734-2016>
- Yoshida GJ. Regulation of heterogeneous cancer-associated fibroblasts: the molecular pathology of activated signaling pathways. *J Exp Clin Cancer Res* 2020; 39(1): 112. <https://doi.org/10.1186/s13046-020-01611-0>
- Louault K, Li RR, DeClerck YA. Cancer-Associated Fibroblasts: Understanding Their Heterogeneity. *Cancers (Basel)* 2020; 12(11): 3108. <https://doi.org/10.3390/cancers12113108>
- Fiori ME, Di Franco S, Villanova L, Bianca P, Stassi G, De Maria R. Cancer-associated fibroblasts as abettors of tumor progression at the crossroads of EMT and therapy resistance. *Mol Cancer* 2019; 18(1): 70. <https://doi.org/10.1186/s12943-019-0994-2>
- Bota-Rabassedas N, Banerjee P, Niu Y, Cao W, Luo J, Xi Y, Tan X, Sheng K, Ahn YH, Lee S, Parra ER, Rodriguez-Canales J, Albritton J, Weiger M, Liu X, Guo HF, Yu J, Rodriguez BL, Firestone JJA, Mino B, Creighton CJ, Solis LM, Villalobos P, Raso MG, Sazer DW, Gibbons DL, Russell WK, Longmore GD, Wistuba II, Wang J, Chapman HA, Miller JS, Zong C, Kurie JM. Contextual cues from cancer cells govern cancer-associated fibroblast heterogeneity. *Cell Rep* 2021; 35(3): 109009. <https://doi.org/10.1016/j.celrep.2021.109009>
- Barrett R, Puré E. Cancer-associated fibroblasts: key determinants of tumor immunity and immunotherapy. *Curr Opin Immunol* 2020; 64: 80-87. <https://doi.org/10.1016/j.coi.2020.03.004>
- Ritchie ME, Phipson B, Wu D, Hu Y, Law CW, Shi W, Smyth GK. limma powers differential expression analyses for RNA-sequencing and microarray studies. *Nucleic Acids Res* 2015; 43(7): e47. <https://doi.org/10.1093/nar/gkv007>
- Friedman J, Hastie T, Tibshirani R. Regularization Paths for Generalized Linear Models via Coordinate Descent. *J Stat Softw* 2010; 33(1): 1-22.
- Therneau TM, Grambsch PM. Modeling survival data: extending the cox model. New York: Springer, 2000.
- Chen B, Khodadoust MS, Liu CL, Newman AM, Alizadeh AA. Profiling Tumor Infiltrating Immune Cells with CIBERSORT. *Methods Mol Biol* 2018; 1711: 243-259. [https://doi.org/10.1007/978-1-4939-7493-1\\_12](https://doi.org/10.1007/978-1-4939-7493-1_12)
- Yue C, Ma H, Zhou Y. Identification of prognostic gene signature associated with microenvironment of lung adenocarcinoma. *PeerJ* 2019; 7: e8128. <https://doi.org/10.7717/peerj.8128>
- Zheng H, Liu H, Li H, Dou W, Wang X. Weighted Gene Co-expression Network Analysis Identifies a Cancer-Associated Fibroblast Signature for Predicting Prognosis and Therapeutic Responses in Gastric Cancer. *Front Mol Biosci* 2021; 8: 744677. <https://doi.org/10.3389/fmolb.2021.744677>
- Chen Z, Zhuo S, He G, Tang J, Hao W, Gao WQ, Yang K, Xu H. Prognosis and Immunotherapy Significances of a Cancer-Associated Fibroblasts-Related Gene Signature in Gliomas. *Front Cell Dev Biol* 2021; 9: 721897. <https://doi.org/10.3389/fcell.2021.721897>
- Matsuda T, Machii R. Morphological distribution of lung cancer from Cancer Incidence in Five Continents Vol. X. *Jpn J Clin Oncol* 2015; 45(4): 404. <https://doi.org/10.1093/jjco/hyv041>
- Song Y, Chen D, Zhang X, Luo Y, Li S. Integrating genetic mutations and expression profiles for survival prediction of lung ade-

- nocarcinoma. *Thorac Cancer* 2019; 10(5): 1220-1228. <https://doi.org/10.1111/1759-7714.13072>
23. Wang F, Li Y, Zhang Z, Wang J, Wang J. SHCBP1 regulates apoptosis in lung cancer cells through phosphatase and tensin homolog. *Oncol Lett* 2019; 18(2): 1888-1894. <https://doi.org/10.3892/ol.2019.10520>
  24. Tao HC, Wang HX, Dai M, Gu CY, Wang Q, Han ZG, Cai B. Targeting SHCBP1 inhibits cell proliferation in human hepatocellular carcinoma cells. *Asian Pac J Cancer Prev* 2013; 14(10): 5645-5650. <https://doi.org/10.7314/apjcp.2013.14.10.5645>
  25. Feng W, Li HC, Xu K, Chen YF, Pan LY, Mei Y, Cai H, Jiang YM, Chen T, Feng DX. SHCBP1 is over-expressed in breast cancer and is important in the proliferation and apoptosis of the human malignant breast cancer cell line. *Gene* 2016; 587(1): 91-97. <https://doi.org/10.1016/j.gene.2016.04.046>
  26. Fischer M, Quaas M, Steiner L, Engeland K. The p53-p21-DREAM-CDE/CHR pathway regulates G2/M cell cycle genes. *Nucleic Acids Res* 2016; 44(1): 164-174. <https://doi.org/10.1093/nar/gkv927>
  27. Zhou C, Wang Y, Lei L, Ji MH, Yang JJ, Xia H. Identifying Common Genes Related to Platelet and Immunity for Lung Adenocarcinoma Prognosis Prediction. *Front Mol Biosci* 2020; 7: 563142. <https://doi.org/10.3389/fmolb.2020.563142>
  28. Gelman IH. Suppression of tumor and metastasis progression through the scaffolding functions of SSeCKS/Gravin/AKAP12. *Cancer Metastasis Rev* 2012; 31(3-4): 493-500. <https://doi.org/10.1007/s10555-012-9360-1>
  29. Tessema M, Belinsky SA. Mining the epigenome for methylated genes in lung cancer. *Proc Am Thorac Soc* 2008; 5(8): 806-810. <https://doi.org/10.1513/pats.200805-045TH>
  30. Jo UH, Whang YM, Sung JS, Kim YH. Methylation of AKAP12{alpha} promoter in lung cancer. *Anticancer Res* 2010; 30(11): 4595-4600.
  31. Park MS, Yang AY, Lee JE, Kim SK, Roe JS, Park MS, Oh MJ, An HJ, Kim MY. GALNT3 suppresses lung cancer by inhibiting myeloid-derived suppressor cell infiltration and angiogenesis in a TNFR and c-MET pathway-dependent manner. *Cancer Lett* 2021; 521: 294-307. <https://doi.org/10.1016/j.canlet.2021.08.015>
  32. Chugh S, Meza J, Sheinin YM, Ponnusamy MP, Batra SK. Loss of N-acetylgalactosaminyltransferase 3 in poorly differentiated pancreatic cancer: augmented aggressiveness and aberrant ErbB family glycosylation. *Br J Cancer* 2016; 114(12): 1376-1386. <https://doi.org/10.1038/bjc.2016.116>
  33. Taniuchi K, Cerny RL, Tanouchi A, Kohno K, Kotani N, Honke K, Saibara T, Hollingsworth MA. Overexpression of GalNAc-transferase GalNAc-T3 promotes pancreatic cancer cell growth. *Oncogene* 2011; 30(49): 4843-4854. <https://doi.org/10.1038/onc.2011.194>
  34. Liu B, Pan S, Xiao Y, Liu Q, Xu J, Jia L. LINC01296/miR-26a/GALNT3 axis contributes to colorectal cancer progression by regulating O-glycosylated MUC1 via PI3K/AKT pathway. *J Exp Clin Cancer Res* 2018; 37(1): 316. <https://doi.org/10.1186/s13046-018-0994-x>
  35. Li L, Mao Y, Zhao L, Li L, Wu J, Zhao M, Du W, Yu L, Jiang P. p53 regulation of ammonia metabolism through urea cycle controls polyamine biosynthesis. *Nature* 2019; 567(7747): 253-256. <https://doi.org/10.1038/s41586-019-0996-7>
  36. Wu G, Zhao Z, Yan Y, Zhou Y, Wei J, Chen X, Lin W, Ou C, Li J, Wang X, Xiong K, Zhou J, Xu Z. *CPS1* expression and its prognostic significance in lung adenocarcinoma. *Ann Transl Med* 2020; 8(6): 341. <https://doi.org/10.21037/atm.2020.02.146>
  37. Pham-Danis C, Gehrke S, Danis E, Rozhok AI, Daniels MW, Gao D, Collins C, Paola JTD, D'Alessandro A, DeGregori J. Urea Cycle Sustains Cellular Energetics upon EGFR Inhibition in EGFR-Mutant NSCLC. *Mol Cancer Res* 2019; 17(6): 1351-1364. <https://doi.org/10.1158/1541-7786.MCR-18-1068>
  38. Zuo S, Wei M, Wang S, Dong J, Wei J. Pan-Cancer Analysis of Immune Cell Infiltration Identifies a Prognostic Immune-Cell Characteristic Score (ICCS) in Lung Adenocarcinoma. *Front Immunol* 2020; 11: 1218. <https://doi.org/10.3389/fimmu.2020.01218>
  39. Saito T, Nishikawa H, Wada H, Nagano Y, Sugiyama D, Atarashi K, Maeda Y, Hamaguchi M, Ohkura N, Sato E, Nagase H, Nishimura J, Yamamoto H, Takiguchi S, Tanoue T, Suda W, Morita H, Hattori M, Honda K, Mori M, Doki Y, Sakaguchi S. Two FOXP3(+)/CD4(+) T cell subpopulations distinctly control the prognosis of colorectal cancers. *Nat Med* 2016; 22(6): 679-684. <https://doi.org/10.1038/nm.4086>
  40. Borst J, Ahrends T, Bąbala N, Melief CJM, Kastenmüller W. CD4+ T cell help in cancer immunology and immunotherapy. *Nat Rev Immunol* 2018; 18(10): 635-647. <https://doi.org/10.1038/s41577-018-0044-0>
  41. Dudeck A, Köberle M, Goldmann O, Meyer N, Dudeck J, Lemmens S, Rohde M, Roldán NG, Dietze-Schwonberg K, Orinska Z, Medina E, Hendrix S, Metz M, Zenclussen AC, von Stebut E, Biedermann T. Mast cells as protectors of health. *J Allergy Clin Immunol* 2019; 144(4S): S4-S18. <https://doi.org/10.1016/j.jaci.2018.10.054>
  42. Kaesler S, Wölbing F, Kempf WE, Skabytska Y, Köberle M, Volz T, Sinnberg T, Amaral T, Möckel S, Yazdi A, Metzler G, Schaller M, Hartmann K, Weide B, Garbe C, Rammensee HG, Röcken M, Biedermann T. Targeting tumor-resident mast cells for effective anti-melanoma immune responses. *JCI Insight* 2019; 4(19): e125057. <https://doi.org/10.1172/jci.insight.125057>
  43. Varricchi G, Galdiero MR, Loffredo S, Marone G, Iannone R, Marone G, Granata F. Are Mast Cells MASTers in Cancer? *Front Immunol* 2017; 8: 424. <https://doi.org/10.3389/fimmu.2017.00424>
  44. Zhang BC, Gao J, Wang J, Rao ZG, Wang BC, Gao JF. Tumor-associated macrophages infiltration is associated with peritumoral lymphangiogenesis and poor prognosis in lung adenocarcinoma. *Med Oncol* 2011; 28(4): 1447-1452. <https://doi.org/10.1007/s12032-010-9638-5>
  45. Kawai O, Ishii G, Kubota K, Murata Y, Naito Y, Mizuno T, Aokage K, Saijo N, Nishiwaki Y, Gemma A, Kudoh S, Ochiai A. Predominant infiltration of macrophages and CD8(+) T Cells in cancer nests is a significant predictor of survival in stage IV non-small cell lung cancer. *Cancer* 2008; 113(6): 1387-1395. <https://doi.org/10.1002/cncr.23712>
  46. Yotsukura M, Asamura H, Suzuki S, Asakura K, Yoshida Y, Nakagawa K, Sakurai H, Watanabe SI, Motoi N. Prognostic impact of cancer-associated active fibroblasts and invasive architectural patterns on early-stage lung adenocarcinoma. *Lung Cancer* 2020; 145: 158-166. <https://doi.org/10.1016/j.lungcan.2020.04.023>
  47. Shimizu K, Kirita K, Aokage K, Kojima M, Hishida T, Kuwata T, Fujii S, Ochiai A, Funai K, Yoshida J, Tsuboi M, Ishii G. Clinicopathological significance of caveolin-1 expression by cancer-associated fibroblasts in lung adenocarcinoma. *J Cancer Res Clin Oncol* 2017; 143(2): 321-328. <https://doi.org/10.1007/s00432-016-2285-2>
  48. Pechkovsky DV, Hackett TL, An SS, Shaheen F, Murray LA, Knight DA. Human lung parenchyma but not proximal bronchi produces fibroblasts with enhanced TGF-beta signaling and alpha-SMA expression. *Am J Respir Cell Mol Biol* 2010; 43(6): 641-651. <https://doi.org/10.1165/rcmb.2009-0318OC>
  49. Huang C, Xu J, Li Z. [Research Progress of Cancer-associated Fibroblasts in Lung Cancer]. *Zhongguo Fei Ai Za Zhi* 2020; 23(4): 267-273. Chinese. <https://doi.org/10.3779/j.issn.1009-3419.2020.102.16>
  50. Richardson AM, Havel LS, Koyen AE, Konen JM, Shupe J, Wiles

- WG 4th, Martin WD, Grossniklaus HE, Sica G, Gilbert-Ross M, Marcus AI. Vimentin Is Required for Lung Adenocarcinoma Metastasis via Heterotypic Tumor Cell-Cancer-Associated Fibroblast Interactions during Collective Invasion. *Clin Cancer Res* 2018; 24(2): 420-432. <https://doi.org/10.1158/1078-0432.CCR-17-1776>
51. Zhou Z, Zhou Q, Wu X, Xu S, Hu X, Tao X, Li B, Peng J, Li D, Shen L, Cao Y, Yang L. VCAM-1 secreted from cancer-associated fibroblasts enhances the growth and invasion of lung cancer cells through AKT and MAPK signaling. *Cancer Lett* 2020; 473: 62-73. <https://doi.org/10.1016/j.canlet.2019.12.039>
  52. Li H, Zhang Q, Wu Q, Cui Y, Zhu H, Fang M, Zhou X, Sun Z, Yu J. Interleukin-22 secreted by cancer-associated fibroblasts regulates the proliferation and metastasis of lung cancer cells via the PI3K-Akt-mTOR signaling pathway. *Am J Transl Res* 2019; 11(7): 4077-4088.
  53. Shintani Y, Fujiwara A, Kimura T, Kawamura T, Funaki S, Minami M, Okumura M. IL-6 secreted from cancer-associated fibroblasts mediates chemoresistance in nscl by increasing epithelial-mesenchymal transition signaling. *J Thorac Oncol* 2016; 11(9): 1482-1492. <https://doi.org/10.1016/j.jtho.2016.05.025>
  54. Lappano R, Talia M, Cirillo F, Rigracciolo DC, Scordamaglia D, Guzzi R, Miglietta AM, De Francesco EM, Belfiore A, Sims AH, Maggolini M. The IL1 $\beta$ -IL1R signaling is involved in the stimulatory effects triggered by hypoxia in breast cancer cells and cancer-associated fibroblasts (CAFs). *J Exp Clin Cancer Res* 2020; 39(1): 153. <https://doi.org/10.1186/s13046-020-01667-y>
  55. Ershaid N, Sharon Y, Doron H, Raz Y, Shani O, Cohen N, Montaran L, Leider-Trejo L, Ben-Shmuel A, Yassin M, Gerlic M, Ben-Baruch A, Pasmanik-Chor M, Apte R, Erez N. NLRP3 inflammasome in fibroblasts links tissue damage with inflammation in breast cancer progression and metastasis. *Nat Commun* 2019; 10: 4375. <https://doi.org/10.1038/s41467-019-12370-8>
  56. Broad RV, Jones SJ, Teske MC, Wastall LM, Hanby AM, Thorne JL, Hughes TA. Inhibition of interferon-signalling halts cancer-associated fibroblast-dependent protection of breast cancer cells from chemotherapy. *Br J Cancer* 2021; 124(6): 1110-1120. <https://doi.org/10.1038/s41416-020-01226-4>
  57. Katanov C, Lerrer S, Liubomirski Y, Leider-Trejo L, Meshel T, Bar J, Feniger-Barish R, Kamer I, Soria-Artzi G, Kahani H, Banerjee D, Ben-Baruch A. Regulation of the inflammatory profile of stromal cells in human breast cancer: prominent roles for TNF-alpha and the NF-kappaB pathway. *Stem Cell Res Ther* 2015; 6(1): 87. <https://doi.org/10.1186/s13287-015-0080-7>
  58. Nakamura H, Ichikawa T, Nakasone S, Miyoshi T, Sugano M, Kojima M, Fujii S, Ochiai A, Kuwata T, Aokage K, Suzuki K, Tsuboi M, Ishii G. Abundant tumor promoting stromal cells in lung adenocarcinoma with hypoxic regions. *Lung Cancer* 2018; 115: 56-63. <https://doi.org/10.1016/j.lungcan.2017.11.013>
  59. Tao LL, Huang GC, Wang R, Pan Y, He ZY, Chu XY, Song HZ, Chen LB. Cancer-associated fibroblasts treated with cisplatin facilitates chemoresistance of lung adenocarcinoma through IL-11/IL-11R/STAT3 signaling pathway. *Sci Rep* 2016; 6: 38408. <http://dx.doi.org/10.1038/srep38408>
  60. Ahmadzadeh M, Rosenberg SA. TGF-beta 1 attenuates the acquisition and expression of effector function by tumor antigen-specific human memory CD8 T cells. *J Immunol* 2005; 174(9): 5215-5223. <https://doi.org/10.4049/jimmunol.174.9.5215>
  61. Feig C, Jones JO, Kraman M, Wells RJ, Deonarine A, Chan DS, Connell CM, Roberts EW, Zhao Q, Caballero OL, Teichmann SA, Janowitz T, Jodrell DI, Tuveson DA, Fearon DT. Targeting CXCL12 from FAP-expressing carcinoma-associated fibroblasts synergizes with anti-PD-L1 immunotherapy in pancreatic cancer. *Proc Natl Acad Sci U S A* 2013; 110(50): 20212-20217. <https://doi.org/10.1073/pnas.1320318110>
  62. Kumar V, Donthireddy L, Marvel D, Condamine T, Wang F, Lavilla-Alonso S, Hashimoto A, Vonteddu P, Behera R, Goins MA, Mulligan C, Nam B, Hockstein N, Denstman F, Shakamuri S, Speicher DW, Weeraratna AT, Chao T, Vonderheide RH, Languino LR, Ordentlich P, Liu Q, Xu X, Lo A, Puré E, Zhang C, Loboda A, Sepulveda MA, Snyder LA, Gabrilovich DI. Cancer-Associated Fibroblasts Neutralize the Anti-tumor Effect of CSF1 Receptor Blockade by Inducing PMN-MDSC Infiltration of Tumors. *Cancer Cell* 2017; 32(5): 654-668. e5. <https://doi.org/10.1016/j.ccell.2017.10.005>
  63. Lakins MA, Ghorani E, Munir H, Martins CP, Shields JD. Cancer-associated fibroblasts induce antigen-specific deletion of CD8 (+) T Cells to protect tumour cells. *Nat Commun* 2018; 9: 948. <https://doi.org/10.1038/s41467-018-03347-0>
  64. Yang N, Lode K, Berzaghi R, Islam A, Martinez-Zubiaurre I, Hellevik T. Irradiated tumor fibroblasts avoid immune recognition and retain immunosuppressive functions over natural killer cells. *Front Immunol* 2020; 11: 602530. <http://dx.doi.org/10.3389/fimmu.2020.602530>
  65. Hudson K, Cross N, Jordan-Mahy N, Leyland R. The extrinsic and intrinsic roles of pd-1l and its receptor pd-1: implications for immunotherapy treatment. *Front Immunol* 2020; 11: 568931. <https://doi.org/10.3389/fimmu.2020.568931>
  66. Huang MY, Jiang XM, Wang BL, Sun Y, Lu JJ. Combination therapy with PD-1/PD-L1 blockade in non-small cell lung cancer: strategies and mechanisms. *Pharmacol Ther* 2021; 219: 107694. <https://doi.org/10.1016/j.pharmthera.2020.107694>
  67. Inoue C, Miki Y, Saito R, Hata S, Abe J, Sato I, Okada Y, Sasano H. PD-L1 Induction by Cancer-Associated Fibroblast-Derived Factors in Lung Adenocarcinoma Cells. *Cancers (Basel)* 2019; 11(9): 1257. <https://doi.org/10.3390/cancers11091257>